

## ORIGINAL ARTICLE

# Lithotrophic iron-oxidizing bacteria produce organic stalks to control mineral growth: implications for biosignature formation

Clara S Chan<sup>1,2</sup>, Sirine C Fakra<sup>3</sup>, David Emerson<sup>4</sup>, Emily J Fleming<sup>4</sup> and Katrina J Edwards<sup>2</sup>  
<sup>1</sup>Department of Marine Chemistry and Geochemistry, Woods Hole Oceanographic Institution, Woods Hole, MA, USA; <sup>2</sup>Departments of Biological Sciences and Earth Sciences, University of Southern California, Los Angeles, CA, USA; <sup>3</sup>Advanced Light Source, Lawrence Berkeley National Laboratory, Berkeley, CA, USA and <sup>4</sup>Bigelow Laboratory for Ocean Sciences, West Boothbay Harbor, ME, USA

**Neutrophilic Fe-oxidizing bacteria (FeOB) are often identified by their distinctive morphologies, such as the extracellular twisted ribbon-like stalks formed by *Gallionella ferruginea* or *Mariprofundus ferrooxydans*. Similar filaments preserved in silica are often identified as FeOB fossils in rocks. Although it is assumed that twisted iron stalks are indicative of FeOB, the stalk's metabolic role has not been established. To this end, we studied the marine FeOB *M. ferrooxydans* by light, X-ray and electron microscopy. Using time-lapse light microscopy, we observed cells excreting stalks during growth (averaging  $2.2\ \mu\text{m h}^{-1}$ ). Scanning transmission X-ray microscopy and near-edge X-ray absorption fine structure (NEXAFS) spectroscopy show that stalks are Fe(III)-rich, whereas cells are low in Fe. Transmission electron microscopy reveals that stalks are composed of several fibrils, which contain few-nanometer-sized iron oxyhydroxide crystals. Lepidocrocite crystals that nucleated on the fibril surface are much larger ( $\sim 100\ \text{nm}$ ), suggesting that mineral growth within fibrils is retarded, relative to sites surrounding fibrils. C and N 1s NEXAFS spectroscopy and fluorescence probing show that stalks primarily contain carboxyl-rich polysaccharides. On the basis of these results, we suggest a physiological model for Fe oxidation in which cells excrete oxidized Fe bound to organic polymers. These organic molecules retard mineral growth, preventing cell encrustation. This model describes an essential role for stalk formation in FeOB growth. We suggest that stalk-like morphologies observed in modern and ancient samples may be correlated confidently with the Fe-oxidizing metabolism as a robust biosignature.**

*The ISME Journal* (2011) 5, 717–727; doi:10.1038/ismej.2010.173; published online 25 November 2010

**Subject Category:** geomicrobiology and microbial contributions to geochemical cycles

**Keywords:** biomineralization; *Gallionella*; *Mariprofundus ferrooxydans*; spectromicroscopy; Zetaproteobacteria

## Introduction

A great challenge in determining the Earth's biological history is finding and confidently identifying traces of ancient organisms, especially geochemically influential microbes that record geobiological clues about the past. Organic, isotopic and morphological biosignatures can give powerful insight into the timing of important biogeochemical processes such as oxygenic photosynthesis and sulfate reduction (Summons *et al.*, 1999; Shen *et al.*, 2001). The ideal biosignature correlates with a particular microbial population and a defined environmental condition, telling us what lived when, and in what

type of paleoenvironment. However, despite the great diversity of known microorganisms, there exist few signatures that resolve specific taxonomic or metabolic groups, greatly limiting our ability to reconstruct the history of life on Earth, and its role in important ecological and biogeochemical processes.

Biomineralization by microbes can form the basis for biosignatures if the mineralogy, texture and/or morphology are specific to a distinct biological group (Banfield *et al.*, 2001). A challenge is that typical microbial shapes are rarely distinctive enough for identification. However, it has been shown that a detailed morphological analysis of certain extant microbes and their corresponding well-preserved microfossils can provide evidence for highly specific identification (for example, microfossils resembling the sulfide oxidizer *Thiomargarita* (Bailey *et al.*, 2007)). For the signature to be robust, the mechanisms and biological relevance of precipitation should be well documented.

Correspondence: CS Chan. Current address: Department of Geological Sciences, University of Delaware, Newark, DE 19716, USA.

E-mail: cschan@udel.edu

Received 14 June 2010; revised 5 October 2010; accepted 5 October 2010; published online 25 November 2010

This is relatively straightforward for intracellular mineralization, which is highly controlled (Bazylnski and Frankel, 2003), but challenging in cases of extracellular precipitation, which can be strongly influenced by environmental chemistry.

One potential candidate for a group-specific biosignature can be found in the distinctive mineralized filamentous extracellular structures produced by neutrophilic Fe-oxidizing bacteria (FeOB). These microbes are common in freshwater and marine environments in which redox gradients of O<sub>2</sub> and Fe(II) exist. They biomineralize extensively because of their metabolic dependence on Fe(II) oxidation combined with the extremely low solubility of Fe(III) at neutral pH. The freshwater Betaproteobacterium *Gallionella ferruginea* has been recognized for nearly two centuries (first described by Ehrenberg in 1836). Recently, the novel (candidate class) Zetaproteobacterium *Mariprofundus ferrooxydans* PV-1 was isolated from Fe(III)-rich microbial mats near Loihi Seamount hydrothermal vents in Hawaii (Emerson and Moyer, 2002; Emerson *et al.*, 2007). These distinct obligate lithoautotrophic FeOB (Hallbeck and Pedersen, 1991; Emerson *et al.*, 2007) produce strikingly similar Fe-rich extracellular twisted stalks, strongly suggesting that stalk formation has a core metabolic role in these Fe oxidizers.

These stalks have been suggestively linked to Fe(III)-rich filaments observed in geological deposits ranging from recent to 1.7 Ga (Alt, 1988; Little *et al.*, 2004; Slack *et al.*, 2007; Hofmann *et al.*, 2008). Fe filaments and stalks could be biosignatures for the presence and activity of FeOB if (1) they are exclusively produced by FeOB; (2) mineralogical and/or morphological criteria are established for Fe microfossil identification; and (3) these structures are linked to Fe-oxidizing metabolism. The first criterion is generally supported, and is based on observations of modern FeOB and on the absence of known biological and chemical processes to create similar Fe-based morphologies (Ghiorse, 1984; Garcia-Ruiz *et al.*, 2003; Hofmann *et al.*, 2008). The second criterion has only been partially met because of limited detailed study of these structures (Hanert, 1999). The third criterion has not yet been proven because the role of these structures in FeOB metabolism is not established. Here, we address the latter two criteria by combining microscopy and spectroscopy techniques to observe *M. ferrooxydans* stalk formation in active cultures and characterize the morphology, physiology, mineralogy, and elemental and organic composition of the stalk. We show that the stalk performs an essential role in eliminating the ferric waste product of Fe-oxidation metabolism by encasing Fe(III) and transporting it away from the cell. Furthermore, we demonstrate that morphological details are rooted in physiology and behavior, and record relevant information pertaining to environmental conditions, making these structures ideal signatures for microaerophilic FeOB.

## Materials and methods

### Culturing

*M. ferrooxydans* PV-1 was grown from frozen stock cultures in artificial seawater (ASW) media, buffered by bicarbonate or 2-(N-morpholino)ethanesulfonic acid to pH of 6–6.5 and FeS as an Fe(II) source (Emerson and Floyd, 2005). Samples for transmission electron microscopy (TEM) and scanning transmission X-ray microscopy (STXM) were prepared in gradient tubes (12 × 75 mm test tube containing 0.5 ml FeS overlain by 3.5 ml ASW, sealed with a silicone stopper and incubated horizontally at ~10° angle). Sample holders (TEM grids and Si<sub>3</sub>N<sub>4</sub> membranes for STXM) were placed on an ACLAR (Ted Pella, Redding, CA, USA) strip in the tube and retrieved after 1 day. Cultures for microtomy were grown as follows: 8 ml of FeS/ASW/1% agarose was overlain by 15 ml ASW in a Petri dish and incubated in a jar with a Campy Pak pouch (BD, Franklin Lakes, NJ, USA). Cultures for time-lapse microscopy were prepared in rectangular microcapillaries (0.2 × 2 mm inner diameter, Vitrocom, Mountain Lakes, NJ, USA). These were filled by capillary action in the following order: ASW media, inoculum and FeS, leaving a small headspace of air; both ends were sealed with Vaseline. The inoculum was PV-1 grown in agarose gradient tubes (ASW with 0.15% low-melt agarose over an FeS/ASW/1% agarose plug). The agarose confined inoculum to the end of the microcapillary, keeping the rest clear. For bulk culture experiments, log-phase cultures of cells were inoculated into Petri dishes containing 20 ml of ASW (10 mM 2-(N-morpholino)ethanesulfonic acid) and Fe(0) (200 mesh; Alfa Aesar, Ward Hill, MA, USA) and grown microaerobically (Emerson and Floyd, 2005). After 21.5 h, cultures were homogenized by repeated pipetting, and analyzed for Fe content, cell number and stalk length.

### Fe measurements

Bulk culture Fe concentrations were determined by the ferrozine method (Stookey, 1970). Aliquots (0.1 ml) of cultures were added to 0.5 M HCl (final concentration). Fe(II) ( $78.7 \pm 6.7 \mu\text{M}$  s.e.) was measured in triplicate with ferrozine (100  $\mu\text{M}$ ) in an acetate buffer (1.4 M) at 562 nm on a Multiskan Microplate Reader MCC/340 (Thermo Scientific, Waltham, MA, USA). Total Fe was measured (in triplicate) by reducing Fe(III) with hydroxyl amine (120 mM) before adding ferrozine. Fe(III) was then calculated as the difference between Fe(II) and total Fe ( $96.5 \pm 4.2 \mu\text{M}$  s.e.).

### Light microscopy

Microcapillary slide cultures were observed using an Olympus BX 60 light microscope (Center Valley, PA, USA), using brightfield and phase contrast methods. For time-lapse studies, images were captured every 5 min with a QIACAM CCD camera and QCapture Pro software (Qimaging, Surrey, BC,

Canada). Cultures were also observed by differential interference contrast (DIC) using a Zeiss AxioImager Z1 light microscope, a Zeiss AxioCam Mrm camera and Axiovision imaging software (Zeiss, Oberkochen, Germany). For cell counting and stalk measurements, bulk culture samples were spread evenly on a 0.5% agarose-coated fluoroslide printed with 10 mm circles (Thermo Scientific) (Emerson and Moyer, 2002). Cells were stained with Syto 13 (Invitrogen, Carlsbad, CA, USA) and counted using fluorescence microscopy ( $1.17 \times 10^9 \pm 2.92 \times 10^7$  cells per l s.e.;  $n = 64$ ). Stalk length ( $31.2 \pm 1.4 \mu\text{m}$  s.e.;  $n = 92$ ) was measured between each stalk bifurcation by tracing each segment with the measure tool in the QCapture Pro software. For each 10 mm circle ( $n = 4$ ), at least 10 fields were examined.

#### Stalk length and Fe calculations

The stalk formation rate was determined by dividing the stalk length produced by one cell from formation to division ( $31.2 \mu\text{m}$  average,  $n = 92$ ) by 12 h, the known doubling time of *M. ferrooxydans* (Emerson *et al.*, 2007). The amount of Fe(II) oxidized per cell was calculated as follows. The total stalk length per volume ( $5.93 \times 10^{10} \mu\text{m l}^{-1}$ ) was divided by the stalk length produced by one cell ( $31.2 \mu\text{m}$ ) to determine the number of individual cells responsible for producing the total stalk mass ( $1.90 \times 10^9$  cells per l). Then, the total Fe(III) concentration ( $1.74 \times 10^{-5} \text{ mol l}^{-1}$ ) was divided by the number of cells ( $1.90 \times 10^9$  cells per l) to determine the amount of Fe oxidized per cell ( $9.16 \times 10^{-15} \text{ mol per cell}$ ). Note that this assumes that all of the Fe(III) was biologically oxidized; the culture time and conditions were controlled such that this assumption would be valid (or nearly so).

#### TEM

Samples for TEM were prepared in three ways: (1) Formvar-coated copper grids were inserted into cultures to preserve the delicate cell-stalk spatial relationships. (Normal handling causes cells to break free of stalks.) The grids were carefully removed, rinsed in distilled water, air-dried and C-coated. (2) Samples were pipetted directly onto grids, rinsed in distilled water, air-dried and C-coated. (3) Samples were dehydrated in a series of solutions of increasing percentages of acetone, embedded in Epon-Araldite resin, ultramicrotomed into 70–100 nm sections and mounted on C-coated, formvar-coated copper grids. Analyses were performed on a Zeiss 10CA TEM (100 kV accelerating voltage), Zeiss Libra 120 PLUS (Zeiss) (120 kV) and Philips (FEI, Hillsboro, OR, USA) CM200 HRTEM (200 kV) with a Link ultrathin-window energy dispersive X-ray detector.

#### STXM

STXM analyses were performed on a sample grown on a  $\text{Si}_3\text{N}_4$  membrane (Silson Ltd., Northampton,

UK), rinsed in distilled water and air-dried. STXM and near-edge X-ray absorption fine structure (NEXAFS) spectroscopy measurements were taken on beamlines 11.0.2 and 5.3.2 of the Advanced Light Source, Lawrence Berkeley National Lab (Kilcoyne *et al.*, 2003). These microscopes use a Fresnel zone plate lens (25 nm outer zones) to focus a monochromatic X-ray beam onto a scanned sample to record transmission images with a scintillator-photomultiplier detector assembly. The imaging contrast relies on core electron excitation by X-ray absorption (Stohr, 1992). X-ray images recorded at energies just below and at the relevant absorption edges were converted into optical density (OD) images and used to derive elemental maps. OD can be expressed for a given X-ray energy from the Beer-Lambert law as  $\text{OD} = -\ln(I/I_0) = \mu\rho t$ , where  $I$ ,  $I_0$ ,  $\mu$ ,  $\rho$  and  $t$  are transmitted intensity through the sample, incident intensity, mass absorption coefficient, density and sample thickness, respectively. NEXAFS spectra from regions of interest were obtained from image sequences (that is, stacks) collected at energies spanning the relevant absorption edge. Beam damage was checked as described by Chan *et al.* (2009) and was not observed. See Supplementary Methods for atomic ratio calculations. At least two different sample regions were analyzed for each element. The theoretical spectral and spatial resolutions were  $\pm 100 \text{ meV}$  and 30 nm, respectively. The photon energy was calibrated at the C 1s edge using the Rydberg transitions of gaseous  $\text{CO}_2$  at 292.74 eV (C 1s  $\rightarrow$  3s ( $\nu = 0$ )) and 294.96 eV (C 1s  $\rightarrow$  3p ( $\nu = 0$ )), at the N 1s edge using the N 1s  $\rightarrow$  3s ( $\nu = 0$ ) transition at 401.1 eV of gaseous  $\text{N}_2$ , at the O 1s edge using the O 1s  $\rightarrow$  3s transition at 538.9 eV of gaseous  $\text{CO}_2$  and at Fe 2p edge using ferrihydrite Fe 2p<sub>3/2</sub> resonance set at 709.5 eV. All data processing was carried out using IDL aXis2000 software (Hitchcock, an IDL-based analytical package, <http://unicorn.mcmaster.ca>).

## Results

#### Correlating stalk formation and cell growth

Microslide cultures enabled visualization of *M. ferrooxydans* cell and stalk growth in opposing gradients of  $\text{O}_2$  and Fe(II). Cell and stalk growth is observed within 1–2 days and continued for a week or longer, consistent with results of test tube gradient cultures (Emerson *et al.*, 2007). A single cell is located at the end of a stalk. Stalk formation begins with attachment (to glass, in this case); the holdfast is characterized by dense mineral precipitation (Supplementary Figure S1a). Cell growth coincides with translocation of the cell, although the stalk remains stationary (Figure 1 and Supplementary Video S1). As cells grow, they rotate, resulting in twisted or coiled stalks. Cell division results in bifurcation, sequential cell division results in multiple branching and cells may leave stalks (see Supplementary Video S2). The



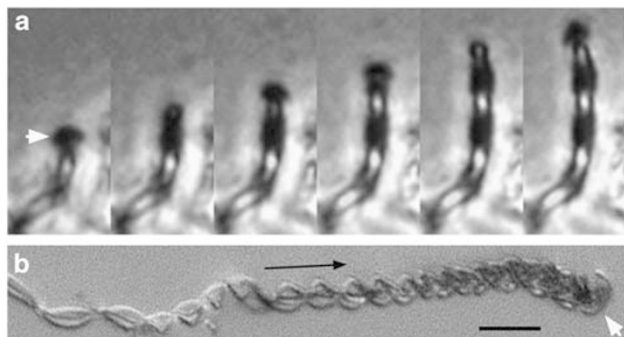


**Figure 1** Light micrographs of *M. ferrooxydans*. (a) Time-lapse series of phase contrast images of a cell creating a twisted stalk in a microslide culture; time interval = 10 min. The image series shows that the cell (white arrow) rotates and moves upward as the stalk is formed. Each image is  $6.4\ \mu\text{m}$  wide (see Supplementary Video S1). (b) Differential interference contrast (DIC)-extended focus light micrograph showing change in stalk width along the length of the stalk. The white arrow points to a curved rod-shaped cell; the black arrow indicates direction of stalk growth. Scale bar =  $10\ \mu\text{m}$ .

cell–stalk connection is fragile; typical handling of samples (for example, pipetting) causes most cells to break away from stalks. Stalk formation is measured between  $0.6$  and  $5.5\ \mu\text{m h}^{-1}$  ( $n = 15$ ), averaging  $2.2\ \mu\text{m h}^{-1}$ . A Petri dish-based liquid culture yielded an average stalk formation rate of  $2.6\ \mu\text{m cell}^{-1}\ \text{h}^{-1}$ , which agrees well with the microslide-based rate. Each cell oxidized  $9.2 \times 10^{-15}$  mol Fe per cell and produced a stalk averaging  $31\ \mu\text{m}$  in length between divisions.

#### Cell–stalk–mineral spatial relationships

The cells are shaped in the form of beans or bent rods; stalk formation occurs within the concavity of the cell. A range of cell lengths and stalk morphologies are observed (Figures 1, 2 and Supplementary Figure S1). Cell lengths varied from  $0.8$  to  $4.7\ \mu\text{m}$  (in TEM), occasionally up to  $11\ \mu\text{m}$  (in microslides). Stalk widths ranged from  $0.3$  to  $1.8\ \mu\text{m}$  (in TEM), occasionally up to  $8\ \mu\text{m}$  wide (in microslides). Smaller cells occur in pairs, attached to the ends of a branched stalk (Supplementary Figure S1c and Video S2). The width of the stalk near the cell correlates with the cell length. The stalk gradually widens from the holdfast to the cell, as illustrated in Figure 1b, Supplementary Figures S1d and S2. The stalks are composed of 2–30 parallel nanometer-sized fibrils. Stalk fibrils are electron dense and sometimes have a smooth, less-electron-dense layer at the ends closest to the cell, at the edges of the fibrils (Figure 2b). At the cell surface, the fibrils are typically thin and widen substantially over the first few  $100\ \text{nm}$  (Figure 2 and Supplementary Figure S1b). Away from the cell, individual fibrils exhibit more subtle increases in width with increasing distance from the cell (Supplementary Figure S3). The number of fibrils increases with increasing stalk width (Figure 1b, Supplementary Figures S1d and S2),

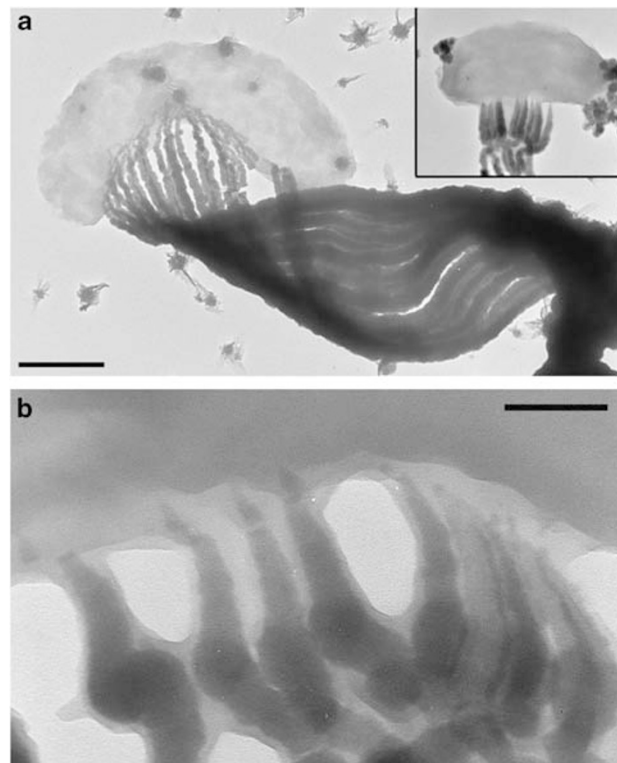


**Figure 2** TEM images of *M. ferrooxydans*. (a) Cell attached to stalk, which is composed of individual filaments. Inset: smaller cell and stalk, displayed at the same scale showing that smaller cells produce narrower stalks with fewer filaments. Scale bar =  $500\ \text{nm}$ . (b) TEM image of the cell–stalk interface, showing that the fibrils taper toward the cell, and are composed of an electron dense core and a lighter coating. Scale bar =  $100\ \text{nm}$ .

with branching of individual fibrils coinciding with increased stalk width.

Whole-mount and ultrathin-sectioned samples examined by HRTEM show that lightly mineralized filaments contain nanometer-sized, poorly crystalline, non-electron diffracting Fe oxyhydroxide minerals (see Supplementary Figure S4a for energy dispersive X-ray spectrum). More highly mineralized filaments are coated in blade-like crystals (Figure 3), and identified as lepidocrocite ( $\text{FeOOH}$ ) by electron diffraction (Supplementary Figure S4b). A section through the stalk shows that these crystals radiate outward from the stalk filaments (Figure 3b). HRTEM imaging of highly mineralized filaments (Figure 3c) reveals few-nanometer-sized minerals embedded within the filaments, which contrast in size to the larger, radiating lepidocrocite crystals. It was not possible to obtain an electron diffraction pattern of the minerals within the fibrils (because of the surrounding lepidocrocite). However, least-square linear combination fitting of an Fe  $1s$  X-ray absorption near-edge structure spectrum collected at the micron scale on a stalk indicates the presence of two-line ferrihydrite in addition to lepidocrocite (Supplementary Figure S5).

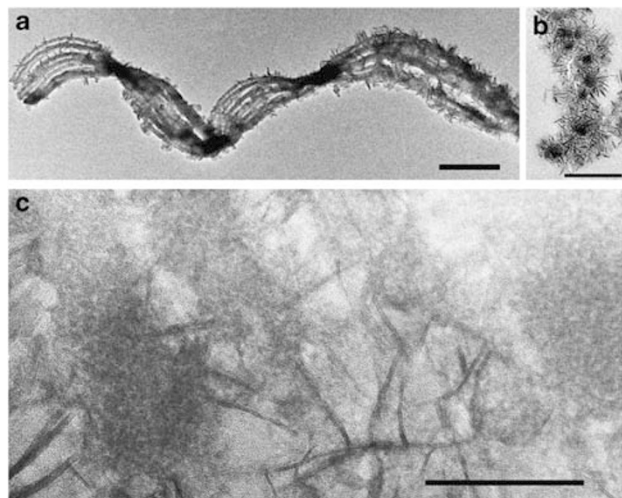


**Figure 3** High-resolution TEM images of mineralized stalks. (a) Whole mount of stalk fragment. Scale bar = 1  $\mu\text{m}$ . (b) Ultrathin section oriented perpendicular to stalk, showing electron-dense core filaments surrounded by radiating crystals of lepidocrocite. Scale bar = 0.5  $\mu\text{m}$ . (c) Oblique section showing filaments containing few-nanometer-sized, granular iron oxyhydroxides surrounded by long, blade-like lepidocrocite (see Supplementary Figure S4 for electron diffraction). Scale bar = 100 nm.

#### Spectromicroscopy of cultured cells and stalks

STXM was used to perform elemental mapping (Figure 4) and NEXAFS spectroscopy at C, N, O 1s and Fe 2p absorption edges on *M. ferrooxydans* cultures (Figure 5 and Supplementary Figure S6). Although both cell and stalk contain C and N, most of the Fe and O are concentrated in the stalk (Figure 4). Surrounding Fe(III)-rich particles (aside from stalks) also exhibited significant C and N levels. Atomic ratios derived from NEXAFS data (Supplementary Table S1) show that the composition of the stalks and particles is similar, whereas the cell is distinct.

C and N spectra (Figure 5 and Supplementary Figure S6, Table 1) show differences in organic functional group distribution between cells and stalks. The C 1s spectrum of the cell is most similar to proteins, as expected, exhibiting a major peak at 288.2 eV, typical of a transition associated with the peptide bond. The major peak in the stalk spectrum is at 288.4 eV, associated with carboxyls or esters (Cody *et al.*, 1998; Boyce *et al.*, 2002); this broad peak lies between (and may include contributions from)  $1s \pi^*_{C=O}$  transitions in acidic polysaccharide carboxyl (288.6 eV) and amide groups in proteins (288.2 eV). The stalk spectrum exhibits a broad shoulder at  $\sim 287.3$  eV, associated with oxygenated groups (Tivanski *et al.*, 2007), aliphatic C and/or aromatic carbonyls/hydroxyls (Myneni, 2002; Brandes *et al.*, 2004; Solomon *et al.*, 2009). The spectrum of surrounding particles is similar to that of the stalk, with a major peak at 288.5 eV, indicative of carboxyls. All sample spectra lack the strong diagnostic  $\pi^*_{C=O}$  peak of carbonate groups ( $\sim 290.2$  eV).

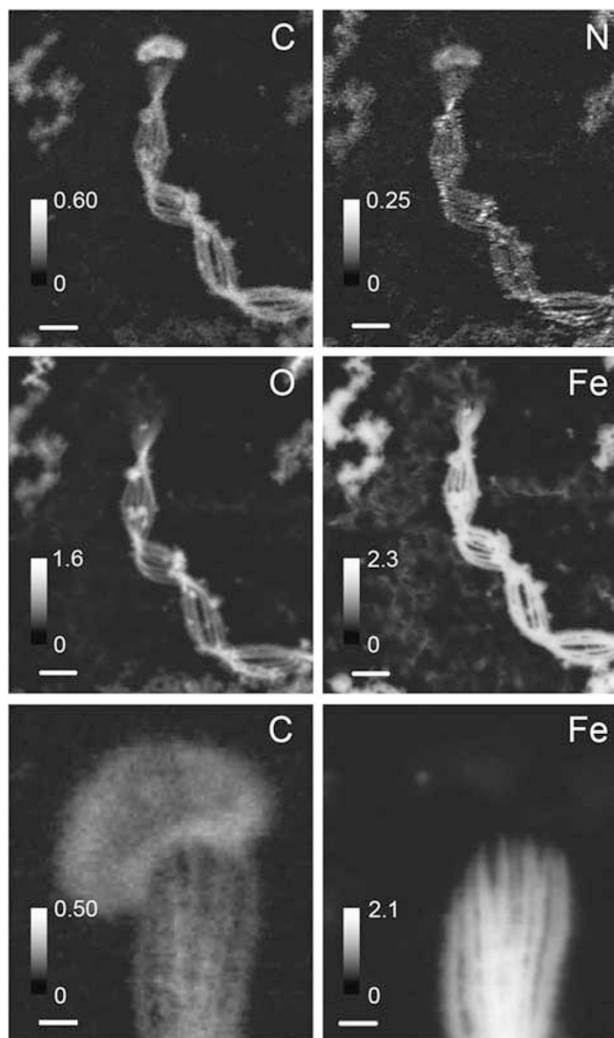


**Figure 4** STXM-derived elemental maps of cells, a stalk and surrounding mineral particles. Intensity scale is in OD units. Scale bars = 1  $\mu\text{m}$  (top four panels), 200 nm (bottom two panels).

The N 1s NEXAFS spectrum (Supplementary Figure S6) of the cell is similar to that of proteins, exhibiting a  $1s \rightarrow \pi^*_{amide}$  transition at 401.2 eV, indicative of peptide bonds, and a  $1s \rightarrow \sigma^*_{N-C}$  broad transition at 406 eV, indicating contributions from lipids and nucleic acids. Stalk and particle spectra are noisy because of low N content; low-intensity  $\pi^*$  transitions observed are consistent with small amounts of protein. The Fe 2p spectra of stalk and particles (Supplementary Figure S6) are similar to those of various Fe(III) oxyhydroxide minerals (Chan *et al.*, 2009 and references therein), whereas the cell spectrum is too noisy (low Fe content) to deduce the Fe chemical state. O spectra (Figure 5) allow some differentiation of FeOOH because of a pre-peak fine structure (530–532 eV) related to the hybridization of Fe 3d and O 2p orbitals (de Groot *et al.*, 1989). The intensity of these pre-peak transitions, occurring from both O 1s and OH 1s core orbitals, has been shown to correlate with the amount of Fe–O–Fe bonds and therefore with

the crystallinity of the sample (Todd *et al.*, 2003). The stalk and particle O 1s spectra are most similar to that of lepidocrocite, consistent with TEM and Fe 1s X-ray absorption near-edge structure results, and do not show significant contributions from organic-associated O. The cell spectrum displays mainly a  $\pi^*_{C=O}$  transition associated with amide groups in proteins (532.1 eV) and no observable Fe(3d)-related transitions, consistent with Fe 2p NEXAFS and mapping results.

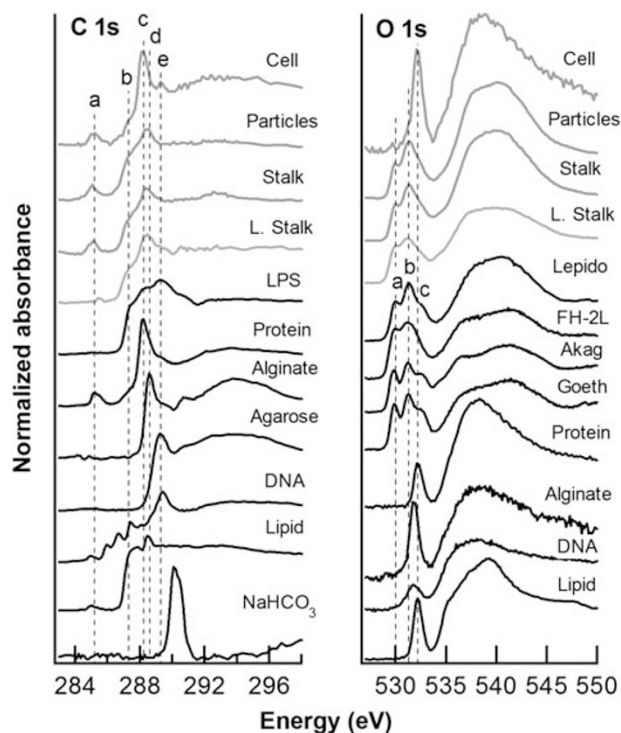


**Figure 5** C and O 1s NEXAFS spectra of *M. ferrooxydans* culture (stalk, cells and surrounding minerals), Loihi microbial mat stalk, and standards. Dashed lines indicate the following energies: 285.2, 287.3, 288.2, 288.6 and 289.3 eV (see Table 1); 529.9, 531.3 and 532.1 eV (O 1s). C standards include *E. coli* lipopolysaccharide (LPS), bovine serum albumin (protein), alginate (acidic polysaccharide), agarose (neutral polysaccharide), DNA and 1,2-dipalmitoyl-sn-glycero-3-phosphoethanolamine (phospholipid). FeOOH standards (phase confirmed by X-ray diffraction) include lepidocrocite, two-line ferrihydrite, akaganeite and goethite. Iron(III) oxyhydroxides exhibit transitions occurring from both O 1s (peaks a and b) and OH 1s (peak c) core orbitals.

**Table 1** Major organic functional groups present in samples and standards

	Energy (eV)	Transition	Functional group	Cell	Particles	Stalk	Loihi stalk
a	285.2	$1s \rightarrow \pi^*_{C=C}$	Unsaturated or aromatic C	x	x	x	
	285.4	$1s \rightarrow \pi^*_{C=C}$	Unsaturated or aromatic C				x
b	287.3	$1s \rightarrow \sigma$	Aliphatic C, aromatic carbonyl, aromatic hydroxyl, other oxygenated groups	x	x	x	x
c	288.2	$1s \rightarrow \pi^*_{C=O}$	Amide (peptide bond)	x			
	288.4–288.5	$1s \rightarrow \pi^*_{C=O}$	Carboxyl, ester		x	x	x
d	288.6	$1s \rightarrow \pi^*_{C=O}$	Carboxyl (polysaccharide)				
e	289.3	$1s \rightarrow \sigma^*$	Alcohol, aliphatic ether	x			
	290.2	$1s \rightarrow \pi^*_{C=O}$	Carbonate				

### Spectromicroscopy of environmental samples

STXM analyses were also performed on twisted stalks in microbial mat samples from the Loihi Seamount in Hawaii (Figure 5, Supplementary Figures S6 and S7). The C 1s NEXAFS spectrum is similar in shape to those of stalk and particles, with a major peak at 288.5 eV, associated with carboxyls. No N was detected. The Fe 2p spectrum is similar to those of Fe oxyhydroxide minerals and the O 1s spectrum is most consistent with ferrihydrite.

### Fluorescent probing of proteins, polysaccharides and lipids

Stalks exhibited poor binding of the protein stain NanoOrange. Six lectins bound stalks to varying degrees, indicating the presence of polysaccharides; one lectin bound poorly (Supplementary Figure S8). Nile red bound cell surfaces (membranes), but not stalks, indicating that stalks are not hydrophobic and thus do not contain lipids.

## Discussion

### The stalk is a record of Fe oxidation metabolism

The time-lapse light microscopy results show that *Mariprofundus* cells rapidly excrete stalks while actively growing. As cells elongate, they excrete wider stalks with more fibrils, suggesting that Fe oxidation and deposition are directly coupled to increases in cell biomass. The stalk bifurcates when a cell divides; each cell then continues producing a stalk that is initially half the width (and presumably half the Fe content) of the original stalk. The cells were not observed to form Fe minerals separate from the stalk, from which we infer that all cell-oxidized Fe is stalk associated. Although non-stalk-shaped Fe-rich particles are observed, it is not clear whether these are biotic (for example, broken pieces of stalk) or abiotic precipitates.

Stalks are rich in Fe(III), whereas cells have a low Fe content (Figure 5), suggesting that the cell is able to localize mineralization outside the cells, thereby avoiding encrustation. The cell C:Fe ratio determined by NEXAFS was  $\sim 100$ . For comparison, Tortell *et al.* (1996) measured C:Fe ratios of  $2.3 \times 10^4$  in non-Fe-limited heterotrophic cultures from the Sargasso Sea. Although Fe is normally a trace



metal in a cell, the Fe content of *Mariprofundus* is relatively high, possibly because of adsorption to the cell surface. On the basis of Fe elemental map and spectra, we conclude that most of the Fe(III) from metabolic Fe oxidation (and abiotic mineralization) is located on the stalk.

#### *Fe-binding organics retard mineral growth in stalk fibrils*

The radiating habit of the lepidocrocite crystals (Figure 3) indicates that they nucleated on the fibril surface and grew outward. Newly formed stalks do not have lepidocrocite, although stalks gain thicker encrustations with time, suggesting that this mineralization ‘overprint’ begins after stalk formation. Fe oxyhydroxide minerals within cultured stalk fibrils are much smaller than the lepidocrocite on the surface, suggesting the presence of a stalk component responsible for retarding crystal growth (including growth associated with transformation). The light smooth coating at the fibril tips possibly represents organic polymers (Figure 2b). The C elemental maps show that stalks indeed contain C throughout the fibrils (Figure 4 and Supplementary Figure S7). The stalk spectrum exhibits peaks similar to biomolecule standards, but lack carbonate, suggesting that C is organic. The dominant 288.4 eV peak ( $\pi^*_{C=O}$ ) is close in energy to the protein amide peak (288.2 eV) and the acidic polysaccharide carboxyl peak (288.6 eV) (Urquhart and Ade, 2002). However, little N is detected in cultured stalks (none in Loihi stalks) and the stalks bind NanoOrange protein stain weakly, from which we conclude that protein could at most account for a small portion of the stalk organic matter. On the basis of C:N ratios, Hallbeck and Pedersen (1995) also concluded that protein is a minor component of the *G. ferruginea* stalk, although there are no studies specifically examining the protein content of stalks. There is also a prominent shoulder at  $\sim 287.3$  eV, similar to the one in the lipid spectrum; however, the stalks do not bind Nile Red, ruling out lipids as a significant component. The stalks do bind several lectins; thus, in light of the above evidence, we conclude that the stalk organic matter is dominated by acidic polysaccharides rich in carboxyls. Previous work on freshwater FeOB systems also found the predominance of acidic polysaccharides associated with Fe-mineralized extracellular structures (Chan *et al.*, 2009). At the circumneutral pH values found in neutrophilic FeOB habitats and in our cultures, these carboxyls would be deprotonated and would have a high affinity for Fe. Further analysis will be required to determine a more specific composition of the organic polymers, as they likely contain variations of our biomolecule standards or may even contain novel components that are not well represented by our reference materials.

Fe(III) occurs throughout the stalk fibrils, not as a coating (Figure 3b); thus, it is an integral part of the stalk. In experiments in which Fe is dissolved, stalks disappear (Emerson *et al.*, 2007).

As a multivalent cation,  $Fe^{3+}$  can crosslink carboxyl-rich polymers; thus, we conclude that stalk fibrils are a matrix of Fe and organics binding one another. Ligands retard mineral growth and it has been suggested by Kennedy *et al.* (2004) and Toner *et al.* (2009) that organics are responsible for the poor crystallinity of microbe-associated Fe minerals. Although we did not quantify the amount of C in the stalk, it appears (in OD units) to be significant, suggesting that these autotrophic organisms expend a significant amount of energy to create the stalk. The necessity of removing waste products and preventing mineral growth near the cell presents a good justification for such an expenditure.

#### *A biomineralization model*

This work demonstrates that the stalk of *M. ferrooxydans* is a well-coordinated biomineral structure controlled by the cell. We combine our results into a model of stalk formation and biomineralization, presented in the following sequence (Figure 6):

- (1) Cells attach to a surface, which may be an existing stalk produced by another cell. Fe is oxidized and excreted from discrete locations on the cell surface, bound to carboxyl groups of organic polymers (for example, acidic polysaccharides). Fe(III) cross-links polymers, aiding in fibril formation. Cells grow, elongate and oxidize more Fe(II), resulting in wider stalks containing more fibrils.
- (2) As cells continue to form new stalk material and move away from older portions of stalks,

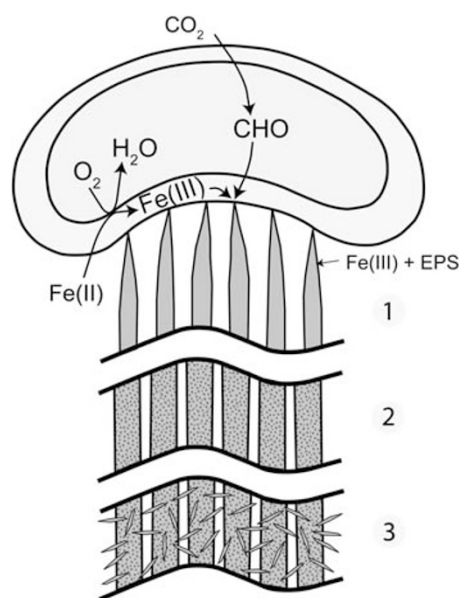


**Figure 6** Model of stalk formation and mineralization process. Iron oxidation is coupled to  $O_2$  reduction (exact location of iron oxidation is not known). (1) Fe(III)-polysaccharide (EPS) is excreted from the cell as fibrils. (2) Over time, Fe(III) precipitates as Fe oxyhydroxides. (3) As stalks age, lepidocrocite nucleates on fibril surfaces.

the Fe(III) in the fibrils precipitates as Fe oxyhydroxide minerals. The timing of precipitation and extent of mineral growth within fibrils have not yet been determined, but our observations and previous studies on environmental samples suggest that they remain nanocrystalline over the timescale of months or longer (Toner *et al.*, 2009).

- (3) As stalks age, Fe oxyhydroxide minerals (for example, lepidocrocite) nucleate on the surfaces of fibrils and grow into larger crystals, whereas the minerals within the fibrils remain small. Abiotic Fe oxidation is typical of FeOB cultures, partly because of autocatalysis of Fe oxidation by the biotic, stalk-bound oxides (Rentz *et al.*, 2007; Druschel *et al.*, 2008). Although minerals inside fibrils could in theory nucleate further mineralization, the limited space within the polymer network would preclude formation of larger crystals.

#### *Physiological implications of stalk formation*

Considering this model, what are the physiological roles of the stalk? The stalk includes a holdfast, which anchors the cell in favorable environmental gradients of O<sub>2</sub> and Fe (II). As the cell excretes the semirigid stalk, the cell translocates away from the holdfast, whereas the stalk remains stationary. In a sense, this provides a form of motility to the cell. A comparable set of functions can be found in sulfur oxidizers *Thiovulum* and *Thioturbo*, which colonize sulfide/O<sub>2</sub> gradient environments with thin, thread-like 'mucous' stalks, forming 'veils' in which conditions are optimal (Fenchel, 1994; Thar and Kuhl, 2002; Muyzer *et al.*, 2005). Similar to *Mariprofundus*, the cells rotate about the axis parallel to the stalk; this rotation has been associated with aerotaxis and fluid mixing. Thar and Kuhl (2003) suggested that cells can sense gradients through a combination of helical motion and sensors located at cell poles. The stalk itself is also used in motility, as the length is controlled to track the position of the oxic/anoxic interface (Thar and Kuhl, 2002).

Perhaps, more importantly, the mineralized stalk serves as an organized structure for depositing solid metabolic products. A similar phenomenon is observed for the sulfur oxidizer *Arcobacter sulfidicus*, which excretes S(0)-rich mineral filaments that form microbial mats (Sievert *et al.*, 2007). Sievert *et al.* suggested that the rapid sulfur filament formation is related to the fact that *A. sulfidicus* lives in extremely high sulfide environments. Thus, the formation of mineralized filaments may be a general adaptation of microbes that rapidly produce large quantities of solid metabolic waste. In the case of *Mariprofundus*, polymers encase and carry Fe(III) away from the cell; in this way, the cell escapes encrustation by its waste products. This model may be generalized to other stalk-forming FeOB, namely,

*G. ferruginea*, and more universally to any FeOB that excrete Fe-mineralized polymers.

Cells that do not normally produce minerals seem to lack such adaptations to prevent cell encrustation (for example, Williams *et al.*, 2005). Although surface and periplasmic precipitation may not completely preclude survival (Miot *et al.*, 2009), it does present a severe challenge, as encrustation would obstruct solute uptake and excretion, and potentially damage the cell wall. Non-structure-forming FeOB, such as microaerophiles *Sideroxydans sp.*, *Ferritrophicum radicolica* and *Gallionella capsiferiformans* (Emerson and Moyer, 1997; Weiss *et al.*, 2007) and the phototroph *Rhodobacter ferrooxidans* (Schädler *et al.*, 2009), likely have less-obvious mechanisms for escaping total encrustation. Minerals may be nucleated on less-organized polymers and periodically shed, or, as Schädler *et al.* (2009) suggest, there may be a combination of local acidification and ligand binding (to keep Fe in solution), as well as cell surface charge adaptations. *Mariprofundus* may use some of these other adaptations in addition to stalk formation.

#### *Supporting the case for an FeOB biosignature*

Despite the abundance of Fe and the significance of its redox state in Earth's history, there is a paucity of biosignatures established for Fe-oxidizing and reducing microorganisms. This limits our ability to piece together the history of Fe biogeochemical cycling, although there is some geochemical and biological evidence that Fe-based metabolisms could have evolved early in Earth's history (Vargas *et al.*, 1998; Johnson *et al.*, 2008; Croal *et al.*, 2009). Fe reducers and anaerobic FeOB (including phototrophs) are not known to form easily distinguishable Fe mineral morphologies, and there have not been any unique organic biomarkers or isotopic signatures established (Kappler and Newman, 2004). Filamentous Fe microfossils corresponding to aerobic stalk-forming FeOB represent the best potential signatures of Fe-cycling microbes thus far. Furthermore, because only aerobic FeOB produce stalks, Fe filaments are indicators of locally oxygenated environments and thus could be important markers of the Earth's oxygen history.

Biosignatures based on morphology are often debated because of the possibility that chemical processes may form similar shapes. This is particularly a problem for microbial signatures because of the small size and simplicity of microbial forms. An often-cited example is a twisted morphology composed of silica and witherite, a barium carbonate (Garcia-Ruiz *et al.*, 2003, 2009). When imaged strategically, this precipitate appears very similar to the twisted stalks of *Gallionella* and *Mariprofundus*, although closer inspection reveals key morphological differences that allow distinction of the chemical precipitates from biological ones. In contrast to the fibrillar, ribbon-like stalks, these chemical



precipitates are rope-like, and emanate from large, clearly abiological aggregates (Figure 1 of Garcia-Ruiz *et al.*, 2003). Furthermore, chemical synthesis of these biomorphs requires environmentally unrealistic conditions and concentrations, inconsistent with what is known about the conditions of Fe oxide deposition. Nevertheless, this work reminds us that abiotic precipitation can result in very biological-looking forms.

In this study of the marine FeOB *M. ferrooxydans* stalk, we have compiled multiple criteria for biosignature distinction that, when considered collectively, delineate them clearly from purely chemical precipitates. We have strengthened its utility as a biosignature by showing that it has vital roles in FeOB metabolism and by linking multiple stalk features (for example, width, branching, twisting and composition) to biological functions. The ultrastructural description can form the basis of morphological criteria for filamentous Fe microfossils. A well-preserved stalk would appear as a twisted or coiled ribbon with a fibrillar substructure; stalks that have undergone recrystallization might lose these details, but width and branching information could still be preserved. As it is a consequence of reproduction and growth—fundamental characteristics of life—multiple branching, especially at regular intervals, would present strong evidence for a biological origin.

The oldest known Fe oxide filaments that may be plausibly linked to FeOB are 1.7 Ga, in the Jerome Jasper (Slack *et al.*, 2007). A careful study of these and other putative Fe microfossils will likely reveal characteristics similar to those observed in *Mariprofundus* stalks. Earth's oceans were once ferruginous, and, as oxygen was produced, it was initially consumed by Fe oxidation (chemical and/or biological) before global oxygenation of the atmosphere and surface oceans, ~2.3–2.4 Ga (Farquhar *et al.*, 2000; Bekker *et al.*, 2004). Such a scenario would be extremely conducive to microaerophilic Fe oxidizers; therefore, the question is whether older filaments exist or, if not, is this an indication that O<sub>2</sub> levels were not high enough to support microbial Fe filament formation before this time? Could these FeOB be the original aerobic microbes, present in localized microaerobic environments before the atmosphere was fully oxygenated? Although we do not have the answers yet, reliable FeOB biosignatures, such as FeOB stalks, will provide a tool to address these fundamental questions.

## Acknowledgements

TEM analyses were performed at the Berkeley National Center for Electron Microscopy, at the Marine Biological Laboratory and at the University of Delaware Bioimaging Facility. We thank Reena Zalpuri (Berkeley) for ultramicrotoming samples, Natalie Villa (University of Delaware) for performing lectin studies and Shawn French

(University of Guelph) for providing LPS standard. We thank T Tylizszczak and ALD Kilcoyne for support at the Advanced Light Source BL11.0.2 and 5.3.2, respectively, and Jill Banfield for helpful discussions. Funding was provided by a NSF Ridge 2000 postdoctoral fellowship (CSC, KJE), by the NSF Microbial Observatories Program (KJE, DE) and by the NASA Astrobiology Institute (KJE, DE). ALS is supported by the Office of Science, Basic Energy Sciences, Division of Materials Science of the United States Department of Energy (DE-AC02-05CH11231).

## References

- Alt JC. (1988). Hydrothermal oxide and nontroite deposits on seamounts in the eastern Pacific. *Mar Geol* **81**: 227–239.
- Bailey JV, Joye SB, Kalanetra KM, Flood BE, Corsetti FA. (2007). Evidence of giant sulphur bacteria in Neoproterozoic phosphorites. *Nature* **445**: 198–201.
- Banfield JF, Moreau JW, Chan CS, Welch SA. (2001). Mineralogical biosignatures and the search for life on Mars. *Astrobiology* **1**: 447–465.
- Bazylinski DA, Frankel RB. (2003). Biologically controlled mineralization in prokaryotes. *Rev Mineral Geochem* **54**: 217–247.
- Bekker A, Holland HD, Wang PL, Rumble D, Stein HJ, Hannah JL *et al.* (2004). Dating the rise of atmospheric oxygen. *Nature* **427**: 117–120.
- Boyce CK, Cody GD, Feser M, Jacobsen C, Knoll AH, Wirick S. (2002). Organic chemical differentiation within fossil plant cell walls detected with x-ray spectromicroscopy. *Geology* **30**: 1039–1042.
- Brandes J, Lee C, Wakeham S, Peterson M, Jacobsen C, Wirick S *et al.* (2004). Examining marine particulate organic matter at sub-micron scales using scanning transmission x-ray microscopy and carbon x-ray absorption near edge structure spectroscopy. *Mar Chem* **92**: 107–121.
- Chan CS, Fakra SC, Edwards DC, Emerson D, Banfield JF. (2009). Iron oxyhydroxide mineralization on microbial extracellular polysaccharides. *Geochim Cosmochim Acta* **73**: 3807–3818.
- Cody G, Ade H, Wirick S, Mitchell GD, Davis A. (1998). Determination of chemical-structural changes in vitrinite accompanying luminescence alteration using C-NEXAFS analysis. *Org Geochem* **28**: 441–455.
- Croal LR, Jiao Y, Kappler A, Newman DK. (2009). Phototrophic Fe(II) oxidation in an atmosphere of H<sub>2</sub>: implications for archean banded iron formations. *Geobiology* **7**: 21–24.
- de Groot F, Grioni M, Fuggle J, Ghijsen J, Sawatzky G, Petersen H. (1989). Oxygen 1s x-ray-absorption edges of transition-metal oxides. *Physical Review B* **40**: 5715–5723.
- Druschel G, Emerson D, Sutka R, Suchecki P, Luther GW. (2008). Low-oxygen and chemical kinetic constraints on the geochemical niche of neutrophilic iron(II) oxidizing microorganisms. *Geochim Cosmochim Acta* **72**: 3358–3370.
- Emerson D, Floyd MM. (2005). Enrichment and isolation of iron-oxidizing bacteria at neutral pH. *Methods Enzymol* **397**: 112–123.
- Emerson D, Moyer C. (1997). Isolation and characterization of novel iron-oxidizing bacteria that grow at

- circumneutral pH. *Appl Environ Microbiol* **63**: 4784–4792.
- Emerson D, Moyer CL. (2002). Neutrophilic Fe-oxidizing bacteria are abundant at the Loihi Seamount hydrothermal vents and play a major role in Fe oxide deposition. *Appl Environ Microbiol* **68**: 3085–3093.
- Emerson D, Rentz JA, Lilburn T, Davis R, Aldrich H, Chan C *et al.* (2007). A novel lineage of Proteobacteria involved in formation of marine Fe-oxidizing microbial mat communities. *PLoS ONE* **2**: e667.
- Farquhar J, Bao H, Thiemens M. (2000). Atmospheric influence of Earth's earliest sulfur cycle. *Science* **289**: 756–758.
- Fenchel T. (1994). Motility and chemosensory behaviour of the sulphur bacterium *Thiovulum majus*. *Microbiology* **140**: 3109–3116.
- Garcia-Ruiz JM, Hyde ST, Carnerup AM, Christy AG, Van Kranendonk MJ, Welham NJ. (2003). Self-assembled silica-carbonate structures and detection of ancient microfossils. *Science* **302**: 1194–1197.
- Garcia-Ruiz JM, Melero-Garcia E, Hyde ST. (2009). Morphogenesis of self-assembled nanocrystalline materials of barium carbonate and silica. *Science* **323**: 362–365.
- Ghiorse WC. (1984). Biology of iron-depositing and manganese-depositing bacteria. *Annu Rev Microbiol* **38**: 515–550.
- Hallbeck L, Pedersen K. (1991). Autotrophic and mixotrophic growth of *Gallionella ferruginea*. *J Gen Microbiol* **137**: 2657–2661.
- Hallbeck L, Pedersen K. (1995). Benefits associated with the stalk of *Gallionella ferruginea*, evaluated by comparison of a stalk-forming and a non-stalk-forming strain and biofilm studies *in-situ*. *Microb Ecol* **30**: 257–268.
- Hanert HH. (1999). The genus *Gallionella*. In: Dworkin M, Falkow S, Rosenberg E, Schleifer K-H, Stackebrandt E (eds). *The Prokaryotes: An Evolving Electronic Resource for the Microbiological Community*. Springer-Verlag: New York.
- Hofmann BA, Farmer JD, Von Blanckenburg F, Fallick AE. (2008). Subsurface filamentous fabrics: an evaluation of origins based on morphological and geochemical criteria, with implications for exopaleontology. *Astrobiology* **8**: 87–117.
- Johnson CM, Beard BL, Roden EE. (2008). The iron isotope fingerprints of redox and biogeochemical cycling in modern and ancient Earth. *Annu Rev Earth Planet Sci* **36**: 457–493.
- Kappler A, Newman DK. (2004). Formation of Fe(III)-minerals by Fe(II)-oxidizing photoautotrophic bacteria. *Geochim Cosmochim Acta* **68**: 1217–1226.
- Kennedy CB, Scott SD, Ferris FG. (2004). Hydrothermal phase stabilization of 2-line ferrihydrite by bacteria. *Chem Geol* **212**: 269–277.
- Kilcoyne ALD, Tyliszczak T, Steele WF, Fakra S, Hitchcock P, Franck K *et al.* (2003). Interferometer-controlled scanning transmission x-ray microscopes at the advanced light source. *J Synchrotron Radiat* **10**: 125–136.
- Little CTS, Glynn SEJ, Mills RA. (2004). Four-hundred-and-ninety-million-year record of bacteriogenic iron oxide precipitation at sea-floor hydrothermal vents. *Geomicrobiol J* **21**: 415–429.
- Miot J, Benzerara K, Obst M, Kappler A, Hegler F, Schädler S *et al.* (2009). Extracellular iron biomineralization by photoautotrophic iron-oxidizing bacteria. *Appl Environ Microbiol* **75**: 5586–5591.
- Muyzer G, Yildirim E, van Dongen U, Kühl M, Thar R. (2005). Identification of '*Candidatus* Thioturbo danicus,' a microaerophilic bacterium that builds conspicuous veils on sulfidic sediments. *Appl Environ Microbiol* **71**: 8929–8933.
- Myneni SCB. (2002). Soft x-ray spectroscopy and spectro-microscopy studies of organic molecules in the environment. *Rev Mineral Geochem* **49**: 485–579.
- Rentz JA, Kraiya C, Luther GW, Emerson D. (2007). Control of ferrous iron oxidation within circumneutral microbial iron mats by cellular activity and autocatalysis. *Environ Sci Technol* **41**: 6084–6089.
- Schädler S, Burkhardt C, Hegler F, Straub KL, Miot J, Benzerara K *et al.* (2009). Formation of cell-iron-mineral aggregates by phototrophic and nitrate-reducing anaerobic Fe(II)-oxidizing bacteria. *Geomicrobiol J* **26**: 93–103.
- Shen Y, Buick R, Canfield DE. (2001). Isotopic evidence for microbial sulphate reduction in the early Archaean era. *Nature* **410**: 77–81.
- Sievert SM, Wieringa E, Wirsén CO, Taylor CD. (2007). Growth and mechanism of filamentous-sulfur formation by *Candidatus* Arcobacter sulfidicus in opposing oxygen-sulfide gradients. *Environ Microbiol* **9**: 271–276.
- Slack JF, Grenne T, Bekker A, Rouxel OJ, Lindberg PA. (2007). Suboxic deep seawater in the late Paleoproterozoic: evidence from hematitic chert and iron formation related to seafloor-hydrothermal sulfide deposits, central Arizona, USA. *Earth Planet Sci Lett* **255**: 243–256.
- Solomon D, Lehmann J, Kinyangi J, Liang B, Heymann K, Dathe L *et al.* (2009). Carbon (1s) NEXAFS spectroscopy of biogeochemically relevant reference organic compounds. *Soil Sci Soc Am J* **73**: 1817–1830.
- Stoher J. (1992). *NEXAFS Spectroscopy*. Springer-Verlag: Berlin, pp 402.
- Stookey LL. (1970). Ferrozine—a new spectrophotometric reagent for iron. *Anal Chem* **42**: 779–781.
- Summons RE, Jahnke LL, Hope JM, Logan GA. (1999). 2-Methylhopanoids as biomarkers for cyanobacterial oxygenic photosynthesis. *Nature* **400**: 554–557.
- Thar R, Kuhl M. (2002). Conspicuous veils formed by vibrioid bacteria on sulfidic marine sediment. *Appl Environ Microbiol* **68**: 6310–6320.
- Thar R, Kuhl M. (2003). Bacteria are not too small for spatial sensing of chemical gradients: an experimental evidence. *Proc Natl Acad Sci* **100**: 5748–5753.
- Tivanski AV, Hopkins RJ, Tyliszczak T, Gilles MK. (2007). Oxygenated interface on biomass burn tar balls determined by single particle scanning transmission x-ray microscopy. *J Phys Chem A* **111**: 5448–5458.
- Todd E, Sherman DM, Purton JA. (2003). Surface oxidation of pyrite under ambient atmospheric and aqueous (pH = 2 to 10) conditions: electronic structure and mineralogy from x-ray absorption spectroscopy. *Geochim Cosmochim Acta* **67**: 881–893.
- Toner BM, Santelli CM, Marcus MA, Wirth R, Chan CS, McCollom T *et al.* (2009). Biogenic iron oxyhydroxide formation at mid-ocean ridge hydrothermal vents: Juan de Fuca Ridge. *Geochim Cosmochim Acta* **73**: 388–403.
- Tortell PD, Maldonado MT, Price NM. (1996). The role of heterotrophic bacteria in iron-limited ocean ecosystems. *Nature* **383**: 330–332.
- Urquhart SG, Ade H. (2002). Trends in the carbonyl core (C 1S, O 1S)  $\pi^*_{C=O}$  transition in the near-edge x-ray

absorption fine structure spectra of organic molecules. *The J Phys Chem B* **106**: 8531–8538.

Vargas M, Kashefi K, Blunt-Harris EL, Lovley DR. (1998). Microbiological evidence for Fe (III) reduction on early Earth. *Nature* **395**: 65–67.

Weiss JV, Rentz JA, Plaia T, Neubauer SC, Merrill-Floyd M, Lilburn T *et al.* (2007). Characterization of neutrophilic Fe(II)-oxidizing bacteria isolated from the

rhizosphere of wetland plants and description of *Ferrotrophicum radicola* gen. nov. sp. nov., and *Sideroxydans paludicola* sp. nov. *Geomicrobiol J* **24**: 559–570.

Williams KH, Ntarlagiannis D, Slater LD, Dohnalkova A, Hubbard SS, Banfield JF. (2005). Geophysical imaging of stimulated microbial biomineralization. *Environ Sci Technol* **39**: 7592–7600.

Supplementary Information accompanies the paper on The ISME Journal website (<http://www.nature.com/ismej>)